Rev. Adv. Mater. Sci. 55 (2018) 61-68

TUNING THE STRUCTURE AND THE MECHANICAL PROPERTIES OF ULTRAFINE GRAIN Al–Zn ALLOYS BY SHORT TIME ANNEALING

E.V. Bobruk[1,2], X. Sauvage[3], A.M. Zakirov[1] and N.A. Enikeev[1,2]

[1]Institute of Physics of Advanced Materials, Ufa State Aviation Technical University, 12 K. Marx str., Ufa 450008, Russia
[2]Laboratory for Mechanics of Bulk Nanostructured Materials, Saint Petersburg State University, 28 Universitetsky pr., Peterhof, Saint Petersburg, 198504, Russia
[3]Normandie Univ, UNIROUEN, INSA Rouen, CNRS, Groupe de Physique des Matériaux, 76000 Rouen, France

Received: December 18, 2017

Abstract. Solid solution treated Al-Zn alloys with different Zn contents (10 and 30 wt.%) have been nanostructured by severe plastic deformation (SPD) via equal-channel angular pressing method. In-situ transmission electron microscopy observations have been used to follow microstructure evolutions upon annealing. It was shown that SPD leads to the precipitation of Zn particles and that this partial solid solution decomposition was more pronounced in the Al-30%Zn alloy. Annealing at temperatures in range of 200 to 250 °C led to visible dissolution of Zn particles in both alloys and to formation of extensive grain boundary segregations of Zn. This approach helped to design short term annealing treatments leading to specific ultrafine grain structures that could be achieved by static annealing on bulk samples. Last, the tensile behavior of these materials has been investigated with a special emphasis on the influence of the strain rate on the yield stress and on the elongation to failure. It is shown that in any case the yield stress is mainly controlled by the grain size, while a low volume fraction of Zn phase leads to a relatively modest ductility.

1. INTRODUCTION

The development of metallic alloys with ultra fine grain structures (UFG) has attracted lots of interest during the past two decades since it offers a new room for enhanced properties. On a mechanical point of view, it is known since a long time that reducing the grain size may lead to a significant increase of the yield stress, following the Hall and Petch law [1,2]. It is also well admitted that superplastic properties for enhanced formability can be achieved only with fine grain structures [3]. It has been demonstrated that UFG structures can be obtained by sintering of fine scale powders [4] or by severe plastic deformation of bulk materials (SPD) [5-8]. A large number of SPD processes has been developed, and the most popular are nowadays Equal Channel Angular Pressing (ECAP) and High Pressure Torsion (HPT). In any case, controlling the final microstructure is challenging as it depends on processing parameters like strain, strain rate, temperature but also on the alloy composition, the initial microstructure, the impurity level [5-9]. Besides, it has been shown that some typical features resulting from SPD may significantly affect the properties like non equilibrium grain boundaries [10,11], precipitate dissolution [12], grain boundary segregation [13,14] or strain induced phase transformations [15]. For example, in the Al-Zn system, our previous experiments have clearly shown that strain induced Zn segregations at grain boundaries

Corresponding author: X. Sauvage, e-mail: xavier.sauvage@univ-rouen.fr

(GBs) significantly enhance the superplastic properties of AlZn alloys [16,17]. Such GB segregations and wetting layers were observed in an Al-30Zn alloy processed by HPT, where only relatively small samples can be produced (typically discs with a diameter of 20 mm). Thus, the first aim of the present work was to try to reproduce a similar structure using ECAP on much larger samples. However, there are very important differences between these two processes: HPT is continuous, it creates a large deformation gradient through the sample and the typical true strain applied is often larger than a hundred; ECAP is not continuous, deformation is more homogeneously applied through the sample and the typical true strain applied is often lower than twenty. It is important to note that unique UFG structures resulting from HPT in the Al-Zn system result from strain induced decomposition of the initial super saturated solid solution [17-19]. ECAP conditions being so different, it is envisioned that the final structure and properties might also be significantly different. Then, to design a larger number of microstructural states, short time annealing treatments have been optimized with the help of in-situ TEM experiments that allow following precipitate coarsening, nucleation or dissolution, but also grain growth and grain boundary segregations.

2. EXPERIMENTAL

The experiments were conducted on two aluminum-based alloys containing 10 and 30 wt.% Zn prepared from high-purity components (5N Al and 5N5 Zn) by vacuum induction melting. Rods Ø18x100 mm have been cut in the cast ingots, then homogenized at 500 °C during 5 h and water quenched to achieve homogeneous solid solutions with equiaxed grains having a mean size of about 130 μm. Then, materials have been severely deformed at room temperature by Equal Channel Angular Pressing with Parallel Channels (ECAP-PC) [20] with a velocity of 6 mm/s. The intersection angle between the parallel channels and the channel connecting them was 110 degrees. A total number of 6 passes have been applied to the material. The strain produced in each ECAP-PC pass being 1.6, then the total cumulative strain induced into samples was 9.6.

Microstructures of deformed alloys were characterized by transmission electron microscopy (TEM). Samples were prepared using standard electropolishing methods (30%vol. HNO3 in methanol, temperature –35 °C, voltage 20 V) and were observed with an ARM200F JEOL microscope operated at 200 kV. Bright field (BF) and high-angle annular dark field (HAADF – collection angles 80 to 300 mrad) images were recorded by scanning transmission electron microscopy (STEM) with a probe size of 0.2 nm and a convergence angle of 34 mrad. In-situ TEM experiments were carried out with a double tilt heating holder (Gatan 652 MA) on which the sample temperature was first increased from room temperature to 100 °C and then by steps of 50 °C up to 250 C. At each temperature change, the new temperature was stabilized in less than one minute and then samples were kept during 15 min at constant temperature before taking pictures and increasing again the temperature.

X-ray diffraction analysis was conducted with the help of the Rigaku Ultima IV diffractometer using Cu Kα radiation at the voltage of 40 kV and current of 30 mA. Lattice parameter values have been derived by Rietlveld refinement technique realized in «Maud» software [21].

Mechanical tensile tests were performed at room temperature on an Instron 8862 machine with flat samples having a gauge length of 4.0 mm, a width of 1.0 m, and a thickness of 0.7 mm. The tensile tests were performed with a strain rate ranging from 10^{-2} to 10^{-4} s^{-1}.

3. RESULTS

3.1. Microstructures and evolution during short time annealing

The initial coarse grain structure has been significantly refined by the ECAP-PC process in both alloys (Figs. 1a and 1c). The grain size ranges from 0.5 to 1 μm in Al-10Zn and from 0.5 to 0.8 μm in Al-30Zn. Besides, the original super saturated solutions have partly decomposed during the ECAP-PC process since nanoscaled Zn precipitates are clearly visible on HAADF images (providing a Z-contrast in Figs. 1b and 1d). These precipitates are located both at GBs and in grain interior with a typical size ranging from 10 to 30 nm in the Al-10Zn alloy and much more numerous and slightly larger from 10 to 40 nm in the Al-30Zn alloy. There are also few Zn precipitates located at GBs and larger in size (more than 50 nm). These observations are consistent with the lattice parameter measurements (Table 1), showing a significant decrease of the amount of Zn in solid solution during processing (from 10 down to 6.0 wt.% in Al-10Zn and from 30 down to 11.2 wt.% in Al-30Zn). Then, assuming that Zn particles do not contain a significant amount of Al [22-23], XRD data indicate that the volume fraction of Zn phase after ECAP-PC is about 2% and 9.5% in Al-10Zn and Al-30Zn respectively.

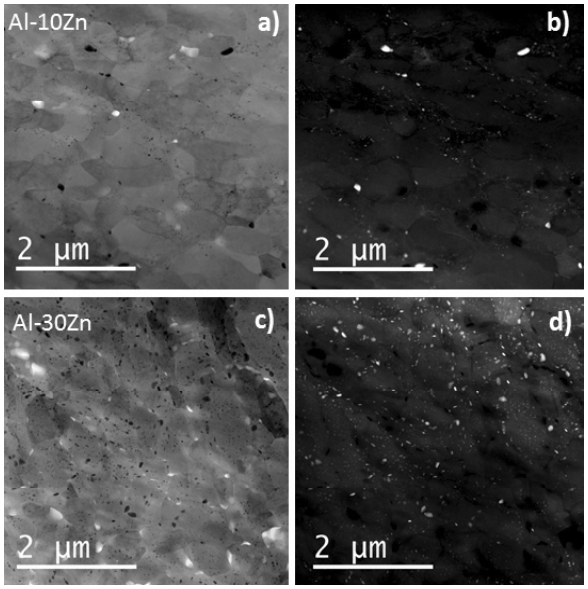

Fig. 1. (a, c) - STEM-BF and (b, d) - STEM-HAADF images showing the microstructure of the (a, b) - Al-10Zn and (c, d) - Al-30Zn alloys after SPD.

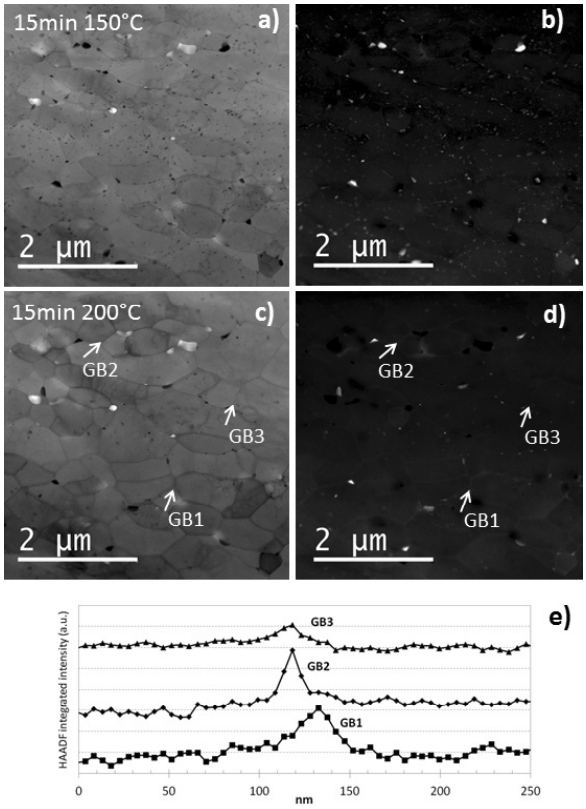

Fig. 2. (a, c) - STEM-BF and (b, d) - STEM-HAADF images showing the evolution of the microstructure of the Al-10Zn alloy processed by SPD followed by 15 min at 150 °C and 15 additional minutes at 200 °C (in-situ annealing showing the same region). (e) Line profiles computed across the three GBs pointed by arrows, and showing a significant increase of the HAADF signal that can be attributed to GB segregation of Zn or wetting layers at 200 °C.

The thermal stability of these microstructures resulting from ECAP-PC has been investigated first thanks to in-situ TEM annealing experiments. For both alloys, the temperature has been progressively increased by steps of 50 °C and images have been recorded at different times. A selection of the most interesting steps is displayed in Fig. 2 (Al-10Zn) and Fig. 3 (Al-30Zn) corresponding to the same locations shown in Fig. 1. Up to 150 °C, no significant change could be observed in the Al-10Zn alloy within the time of the experiment but after 15 min at 150 °C, the number density of Zn precipitates has clearly increased while already existing precipitates have coarsen (Figs. 2a and 2b). However, when the temperature is further increased up to 200 °C, most of particles dissolve (Figs. 2c and 2d) and a significant amount of Zn could be detected along GBs (Fig. 2e). Last important feature, within the temperature range and time investigated here, the grain size is relatively stable and only recovery of subgrains or dislocations occurred. A similar heating ramp has been applied to the Al-30Zn alloy (Fig. 3). The volume fraction of Zn phase is still large at 200 °C and

Table 1. Lattice parameter (a) of the fcc Al matrix measured by XRD in the two alloys after ECAP and after ECAP followed by static annealing (SA) of 10min at 200 °C for Al-10Zn and at 250 °C for Al-30Zn. The Zn content in solid solution (C^{Zn} in SS) was estimated using as reference pure Al with a lattice parameter 0.40509 nm and assuming that 1 wt.% Zn decreases this lattice parameter by 0.00375nm [31]. The volume fraction of particle (F_v) was estimated from mass balance and assuming that Zn particles do not contain a significant amount of Al in solid solution. Corresponding XRD profiles are provided in appendix.

	Al-10Zn ECAP	Al-10Zn ECAP + SA	Al-30Zn ECAP	Al-30Zn ECAP + SA
a (nm)	$0.404867 \pm 2 \times 10^{-6}$	$0.404870 \pm 2 \times 10^{-6}$	$0.404669 \pm 6 \times 10^{-6}$	$0.404520 \pm 4 \times 10^{-5}$
C^{Zn} in SS (wt.%)	6.0 ± 0.2	5.9 ± 0.2	11.2 ± 0.7	15.2 ± 0.5
F_v Zn particles (%vol)	2	1.5	9.5	7.5

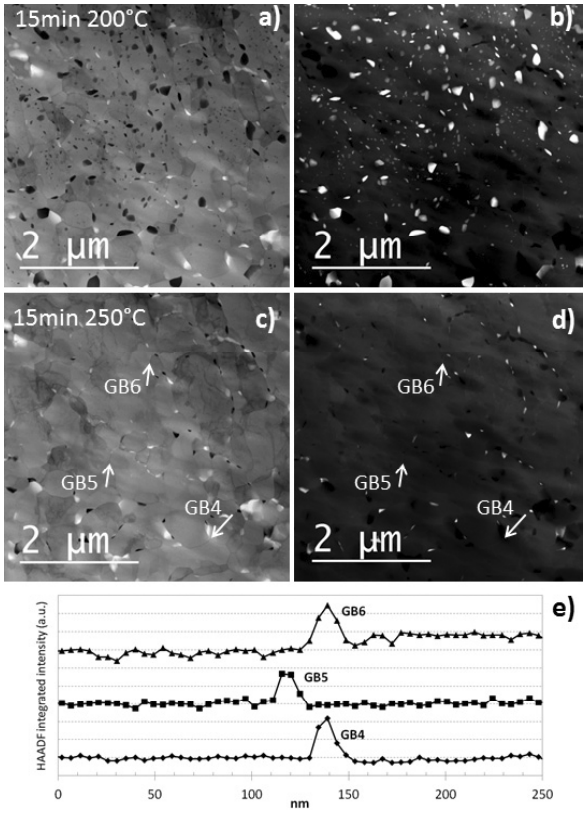

Fig. 3. (a, c) - STEM-BF and (b, d) - STEM-HAADF images showing the evolution of the microstructure of the Al-30Zn alloy processed by SPD followed by 15 min at 200 °C and 15 additional minutes at 250 °C (in-situ annealing showing the same region). (e) Line profiles computed across the three GBs pointed by arrows, and showing a significant increase of the HAADF signal that can be attributed to GB segregation of Zn or wetting layers at 250 °C.

particles have significantly grown (Fig. 3b). At 250 °C, most of particles quickly dissolved, without significant grain growth within the observation time of the experiment (Fig. 3d).

To check if the microstructures observed during in-situ TEM observations could be reproduced by static annealing, bulk pieces of the Al-10Zn and Al-30Zn alloys processed by ECAP-PC have been annealed respectively at 200 and 250 °C during 10 min. The resulting microstructures are displayed in Fig. 4. For the Al-10Zn (Figs. 4a and 4b), grains are relatively equi-axed with a mean size of about 0.8 μm and most of particles have dissolved. These observations are confirmed by XRD data that show a significant change in lattice parameter attributed to an increase of Zn in solid solution (Table 1). However, it is interesting to note that GBs are not covered by Zn segregations or wetting layers (Fig. 4b). Instead, Zn particles have obviously nucleated and

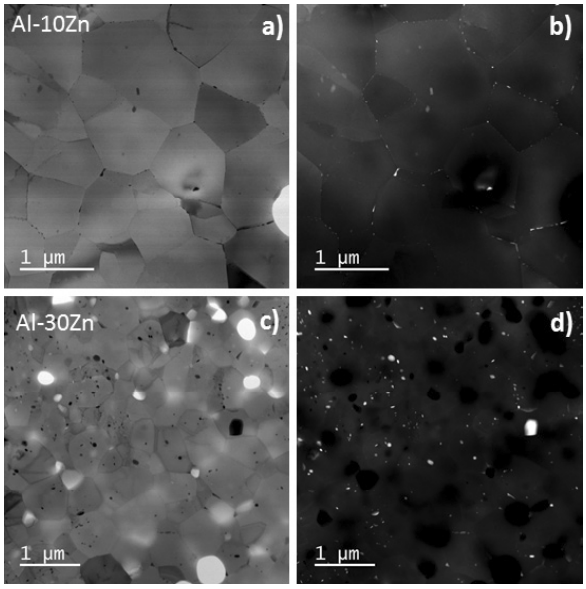

Fig. 4. (a, c) - STEM-BF and (b, d) - STEM-HAADF images showing the microstructure of the: (a, b) - Al-10Zn after SPD followed by static annealing at 200 °C during 10 min and (c, d) - Al-30Zn after SPD followed by static annealing at 250 °C during 10 min.

grown during the sample cooling. The Al-30Zn alloy statically annealed at 250 °C exhibits a grain size in a range of 0.5 to 0.8 μm with a significant remaining volume fraction of Zn particles (Fig. 4d). Nevertheless, XRD data confirm a significant increase of Zn in solid solution and a decrease of this volume fraction as compared to the as-deformed state (Table1).

3.2. Influence of the strain rate and of the Zn content on mechanical properties

The mechanical properties of four different states corresponding to both alloys in the as-ECAP condition and after short time static annealing (10 min 200 °C for Al-10Zn and 10 min 250 °C for Al-30Zn) were investigated. A special emphasis was given on the influence of the strain rate since Al-Zn alloys with UFG structures are potential interesting candidates for superplastic forming [3,24]. The measured yield stresses are plotted in Fig. 5 as a function of the strain rate. It clearly shows that in general, the Al-30Zn alloy exhibits a higher yield stress than the Al-10Zn alloy (10 to 20% higher). In all cases, the short time static annealing led to a decrease of the yield stress (between 10 and 20% depending of the strain rate), and a positive strain rate sensitivity of the yield stress is exhibited. It is however interest-

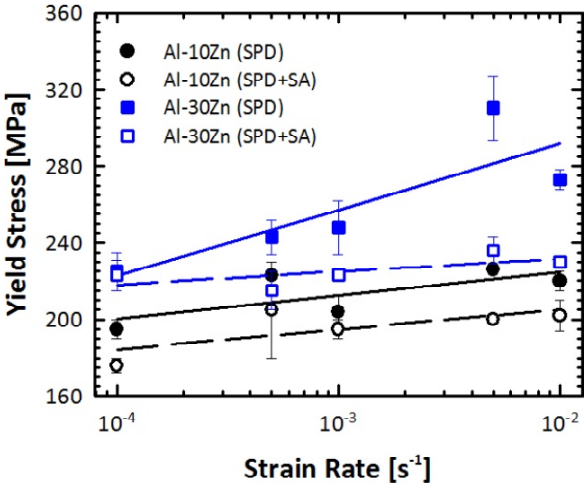

Fig. 5. Strain rate dependence of the yield stress of ultrafine grain Al-Zn alloys after severe plastic deformation (SPD) and after SPD followed by static annealing (SA) of 10 min at 200 °C for Al-10Zn and 10 min at 250 °C for Al-30Zn.

ing to note that this sensitivity is particularly high for the Al-30Zn alloy after SPD and near zero if a short static annealing is applied. Then, regarding the elongation to failure (Fig. 6), differences are not significant between the four different states, excepted for the Al-30Zn after SPD and short time static annealing. The elongation to failure of all other states exhibits a negative strain rate sensitivity with a value of 20-25% at a strain rate of 10^{-4} going down to 15-20% at a strain rate of 10^{-3}. The Al-30Zn exhibits a quite specific behavior with a positive strain rate sensitivity with an elongation to failure up to 35-40% at the highest strain rates.

4. DISCUSSION

4.1. Influence of the Zn content and of the processing route on the UFG structure

The grain size achieved by ECAP-PC in the Al-10Zn alloy ranges from 0.5 to 1 μm which is slightly larger than in the Al-30Zn where it ranges between 0.5 and 0.8 μm (Fig. 1). Such an influence of the Zn content has also been reported in similar alloys processed by HPT [25,26]. This could be attributed to a lower rate of dynamic recovery of defects (especially dislocations) due to Zn atoms in solid solution but it is also most probably the result of the largest number density of Zn particles that nucleate mainly at triple lines and GBs, as they might significantly reduce the GB mobility. Indeed, even if the started structures before ECAP-PC are fully homogeneous solid solutions and if the severe plastic deformation process was carried out at room temperature where the atomic mobility of Zn in Al is negligible [23], in both alloys some Zn particles could be observed within the UFG structure (Fig. 1). It means that some strain induced phase separation (i.e. nucleation and growth of Zn phase) occurred. Such a phenomenon has already been reported during HPT processing of similar Al-Zn alloys [17-18,25,26] and also in the Al-Cu system [15] and is connected with the high density of crystalline defects created during the deformation such as vacancies, dislocations and boundaries. The decomposition is more pronounced in the Al-30Zn alloy due to the higher driving force that is linked to the supersaturation which is the composition difference between the solid solution and the solubility limit given by the phase diagram. This obviously leads to a lower nucleation barrier in the Al-30Zn alloy. As reported for HPT [26], it seems that the solid solution decomposition did not occur through discontinuous precipitation [22] but via heterogeneous precipitation on defects (especially GBs and dislocations) in both alloys. Thus, the mechanisms should be close to those operating during HPT [26,15], but here the solid solution is not fully decomposed because the level of deformation achieved by ECAP-PC is significantly smaller than during HPT. It is however remarkable that no GB segregations or wetting layer of Zn could be observed in the Al-Zn alloys processed by ECAP-PC while it is a quite common feature for similar alloys processed by HPT [17-19,25,26]. This difference might be attributed to the lower level of deformation that reduces the collection of Zn by GBs.

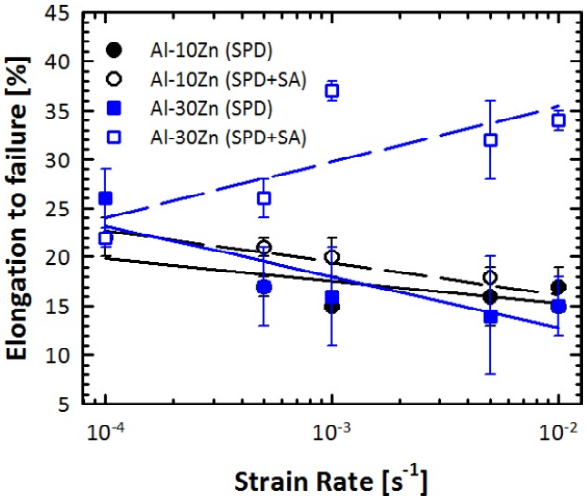

Fig. 6. Strain rate dependence of the elongation to failure of ultrafine grain Al-Zn alloys after severe plastic deformation (SPD) and after SPD followed by static annealing (SA) of 10 min at 200 °C for Al-10Zn and 10 min at 250 °C for Al-30Zn.

4.2. Evolution of UFG structures achieved by ECAP-PC upon short time annealing

In-situ TEM measurements clearly revealed that during heating of the Al-10Zn alloy, the Zn particle volume fraction first increases at about 150 °C and then strongly decreases near 200 °C (Fig. 2). This is connected to the atomic mobility of Zn that becomes high enough near 150 °C [23], and that can promote the full decomposition of the super saturated solid solution. However, when the temperature is further increased up to 200 °C, the equilibrium solubility of Zn in fcc Al becomes large enough [27] and most of particles dissolve. In the Al-30Zn alloy, similarly the phase separation and the particle growth is promoted as soon as the atomic mobility of Zn is high enough (i.e. temperature higher than 150 °C) but the dissolution of particles is delayed to higher temperatures (significant near 250 °C, see Fig. 3) because of the higher solubility limit linked with the higher Zn content of the alloy [27]. Besides, it is interesting to note that within the temperature range and time investigated here, the grain size remains relatively stable (mainly recovery of subgrains or dislocations occurred) in both alloys. Thus, the grain growth is probably limited due to GB pinning by Zn particles when they exist at the lowest temperature and by Zn GB segregations or wetting layers [28] that appear in both alloy at higher temperature concomitantly with particle dissolution (Figs. 2e and 3e).

It is however important to note that such in-situ TEM experiments do not necessarily reflect the equilibrium state because of the very short annealing time but also because of the thermal inertia of the TEM sample, and of the accuracy of the heating stage temperature control. These observations demonstrate however that short time annealing treatments can be used to tune the volume fraction of the Zn phase and to promote GB segregations while keeping a UFG structure. Nevertheless, it is important to note that observations of microstructures after short time static annealing exhibit few differences comparing to in-situ experiments (Fig. 4). In both alloys, after static annealing the grains look more equi-axed and slightly larger in size. This feature might be attributed to the influence of the top and bottom surfaces of the TEM thin foil that may reduce the GB mobility. Another important difference is that after static annealing GBs are not covered by Zn segregations or wetting layers but during the sample cooling Zn particles have obviously nucleated instead. The high driving force for phase separation combined with the high local Zn concentration and GBs acting as nucleation site probably makes precipitation extremely difficult to avoid. However, surprisingly, after HPT such GB segregations or wetting layers are relatively stable and could usually be observed at room temperature [16-19,25,26]. Then, it is believed that it might be the result of the special structure of GBs directly formed by SPD [5-8,11], while in the present case some structural relaxation occurred during the short time annealing making such segregation or wetting layers less stable.

4.3. Relationship between UFG structures achieved by ECAP-PC and mechanical properties

In the four states investigated in the present study, several important structural features may affect the mechanical response, namely the amount of Zn in solid solution, the dislocation density, the grain size and inter-granular Zn precipitates. Typical Hall Petch slopes [2,3] reported for aluminium are near 1.3 MPa $mm^{-1/2}$ [29], which gives a contribution to the yield stress of about 210 MPa (respectively 150 MPa) for a grain size of 0.5 μm (respectively 1 μm). With most of experimental yield stress values lying between 170 and 270 MPa for grain sizes ranging from 0.5 to 1 mm, it clearly indicates that GBs provide the main hardening contribution.

The contribution of Zn solid solutions have been investigated by J. Dash and M. E. Fine [30]. They have shown that the yield stress of aluminum increases of about 5 MPa per atomic percent of Zn in solid solution. In the present situation, it makes a maximum possible contribution of about 75 MPa for the Al-30Zn alloy (15 at.% Zn). But if one compares the yield stress of Al-10Zn and Al-30Zn after short time static annealing where similar grain sizes, negligible volume fraction of intergranular precipitates and low dislocation density were achieved, then the 5 to 10 wt.% Zn difference (i.e. about 2.5 to 5 at.%) in solid solution (see Table 1), may account for most of the difference in yield stress (20-50 MPa). It also clearly indicates that the drop in yield stress after the static annealing of the Al-10Zn alloy (10-20 MPa) might be almost exclusively attributed to the small grain growth reported from TEM observations (Figs. 1a and Fig. 4a) since the change in Zn amount in solid solution is only of 0.5 wt.% (Table 1) which gives a negligible contribution. Precipitation hardening is known to be relatively weak in Al-Zn alloys [31] and in any case, in the investigated states the number density of intergranular precipitate is rela-

tively small, providing then a negligible contribution. However, it is interesting to note that the yield stress of the Al-30Zn as-processed by ECAP-PC exhibits a much stronger strain rate sensitivity. This might be attributed to the higher number density of nanoscaled Zn rich particles and higher Zn content in solid solution (as compared to the Al-10Zn for example) that pin dislocations and inhibit dynamic recovery processes.

Last, the present UFG structures resulting from ECAP-PC exhibit a much lower ductility than those resulting from HPT of the same alloys [17,32]. The elongation to failure of all states exhibits a relatively classical negative strain rate sensitivity due to reduced dynamic recovery at higher strain rate. The Al-30Zn alloy processed by ECAP-PC and followed by static annealing is however an exception with a reverse trend. Interestingly the yield stress of this state exhibits a very low strain rate sensitivity (Figs. 5 and 6) which might lead to a delayed strain localization and damage at higher strain rate. However, none of the structures obtained by ECAP-PC (with or without short time annealing) exhibits superplastic properties which is probably the most striking difference with Al-30Zn UFG structures obtained by HPT [16]. This feature might be attributed to the relatively small size and low volume fraction of Zn particles and the resulting low fraction of Al/Zn interphase boundaries that play a key role in GB sliding mechanisms [3,33].

5. CONCLUSIONS

1) Microstructure evolution upon annealing and mechanical response of UFG Al-10%Zn and Al-30% alloys produced by ECAP was studied. It was shown that severe plastic deformation leads to notable solid solution decomposition which was more pronounced in the case of Al-30%Zn alloy. The precipitates were found to be located both at GBs and in grain interior with a typical size ranging from 10 to 30 nm in the Al-10%Zn alloy and much more numerous and slightly larger from 10 to 40 nm in the Al-30%Zn alloy. It is worthy noting that no grain boundary segregations of Zn or wetting layers have been revealed in these as-processed ECAP samples.

2) Annealing at temperatures of 200-250 °C during in-situ STEM observations resulted in visible dissolution of Zn particles in both alloys as well as formation of grain boundary segregations without significant grain growth. Similar structures were obtained by short time static annealing. GB segregations or wetting layers could however not be preserved at room temperature, they led to the nucleation of nanoscaled Zn particles.

3) Short time static annealing treatments led to a decrease of the yield stress with positive strain rate sensitivity in all studied alloys. Interestingly, the sensitivity is particularly high for the Al-30Zn alloy after SPD and near zero if a short static annealing is applied. The Al-30Zn also exhibits a quite specific behavior with a positive strain rate sensitivity with an elongation to failure up to 35-40% at the highest strain rates.

4) In any case, it is shown that for all ultrafine structures produced from the Al-Zn alloys, the yield stress is mainly controlled by the grain size, while the solid solution, precipitates and the dislocation density play a minor role. Interestingly, these structures did not show however a tendency to demonstrate superductile behavior unlike the same alloys produced by HPT. This feature is attributed to the relatively low volume fraction of Zn particles and the resulting low fraction of Al/Zn interphase boundaries that play a key role in GB sliding mechanisms.

5) Anyway, short term annealing proved to be a fine tuning tool to manipulate structural features in UFG aluminum alloys. In-situ TEM studies are of great help to design such treatments since they allow a quantitative measurements of grain size evolution, precipitate nucleation or dissolution, evolution of defect density and more generally of the distribution of alloying elements (including GB segregations).

ACKNOWLEDGEMENTS

TEM experiments were carried out on the GENESIS facility which is supported by the R?gion Normandie, the M?tropole Rouen Normandie, the CNRS via LABEX EMC3 and the French National Research Agency as a part of the program “Investissements d’avenir” with the reference ANR-11-EQPX-0020. EBSD analyses were conducted on the equipment of the Interdisciplinary Resource Centre for Nanotechnology of Saint Petersburg State University. EB and NE acknowledge the support from Saint Petersburg State University via Lot 2017 Applied (Id:26130576).

REFERENCES

[1] C. Pande and K. Cooper // *Prog. Mater. Sci*. **54** (2009) 689.
[2] F. Louchet, J. Weiss and T. Richeton // *Phys. Rev. Lett*. **97** (2006) 75504.
[3] P. Shariat, R. B. Vastava and T. G. Langdon // *Acta Metallurgica* **30** (1982) 285.
[4] R.W Hayes, David Witkin, Fei Zhou and E.J. Lavernia // *Acta Materialia* **52**. 14 (2004) 4259.

[5] R. Z. Valiev, R. K. Islamgaliev and I. V. Alexandrov // *Prog. Mater. Sci*. **45** (2000) 103.
[6] R. Z. Valiev // *Mater. Sci. Forum* **584-586** (2008) 22.
[7] Y. Estrin and A. Vinogradov // *Acta Materialia* **61** (2013) 782-817.
[8] R. Z. Valiev and T. G. Langdon // *Prog. Mater. Sci*. **51** (2006) 881.
[9] H.W. Zhang, X. Huang, R. Pippan and N. Hansen // *Acta Mater* **58** (2010) 1698.
[10] J. Hu, Y. N. Shi, X. Sauvage, G. Sha and K. Lu // *Science* **355** (2017) 1292.
[11] X. Sauvage, G. Wilde, S. V. Divinski, Z. Horita and R. Z. Valiev // *Mater. Sci. Eng. A* **540** (2012) 1.
[12] X. Sauvage and Y. Ivanisenko // *J. Mater. Sci.* **42** (2007) 1615.
[13] X. Sauvage, N. Enikeev, R. Valiev, Y. Nasedkina and M. Murashkin // *Acta Materialia* **72** (2014) 125.
[14] X. Sauvage, A. Ganeev, Y. Ivanisenko, N. Enikeev, M. Murashkin and R. Valiev // *Adv. Eng. Mat.* **14** (2012) 968.
[15] Y. Nasedkina, X. Sauvage, E. Bobruk and M. Murashkin // *Journal of Alloys and Compounds* **710** (2017) 736.
[16] N. Q. Chinh, R. Z. Valiev, X. Sauvage, G. Varga, K. Havancsák, M. Kawasaki, B. B. Straumal and T. G. Langdon // *Adv. Eng. Mater.* **16** (2014) 1000.
[17] N.Q. Chinh, P.Jenei, J. Gubicza, E.V. Bobruk, R.Z. Valiev and T.G. Langdon // *Materials Letters* **186** (2017) 334.
[18] B. B. Straumal, B. Baretzky, A. A. Mazilkin, F. Philipp, O. A. Kogtenkova, M. N. Volkov and R .Z. Valiev // *Acta Mater.* **52** (2004) 4469.
[19] B. B. Straumal, X. Sauvage, B. Baretzky, A. A. Mazilkin and R. Z. Valiev // *Scripta Mater.* **70** (2014) 59.
[20] G.I. Raab // *Materials Science and Engineering A* **410-411** (2005) 230.
[21] L. Lutterotti // *Nucl. Instr. Meth. Phys. Res. B* **268** (2010) 334.
[22] C. F. Yang, G. Sarkar and R. A. Fournelle // *Acta Metall.* **36** (1988) 1511.
[23] Y.W. Cui, K. Oikawa, R. Kainuma and K. Ishida // *Journal of Phase Equilibria and Diffusion* **27.4** (2006) 333.
[24] P. Kumar, M. Kawasaki and T.G. Langdon // *J Mater Sci* **51** (2016) 7.
[25] E.V. Bobruk, X. Sauvage, N.A. Enikeev, B.B. Straumal and R.Z. Valiev // *Reviews on Advanced Materials Science* **43** (2015) 14.
[26] X. Sauvage, M.Yu. Murashkin, B.B. Straumal, E.V. Bobruk and R.Z. Valiev // *Adv. Eng. Mater.* **17** (2015) 1821.
[27] K. G. Satyanarayana // *Journal of Materials Science* **16** (1981) 1233.
[28] A. R. Kalidindi and C. A. Schuh // *Acta Materialia Volume* **132** (2017) 128-137.
[29] J.W. Wyrzykowski and M.W. Grabski // *Phil. Mag*. **53** (1986) 505.
[30] J. Dash and M. E. Fine // *Acta Metall*. **9** (1961) 149.
[31] J. Dutkiewicz, A. M. Zahra and C. Y. Zahra // *Journal of Materials Science* **27** (1992) 3032.
[32] *Aluminum: Properties and Physical Metallurgy*, ed. by J. E. Hatch (ASM Intlnl, 1984).
[33] K. Edalati, T. Masuda, M. Arita, M. Furui, X. Sauvage, Z. Horita and R.Z. Valiev // *Scientific Reports* **7** (2017) 2662.

Appendix. XRD patterns of Al-10Zn and Al-30Zn alloys

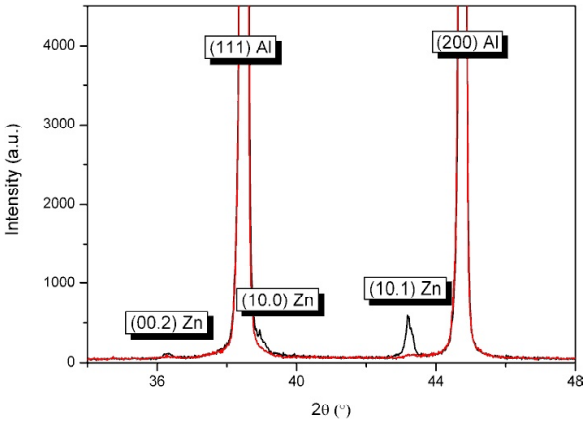

Fig. A1. XRD profiles of the Al-10Zn alloy after ECAP (black line) and after ECAP+SA (red line).

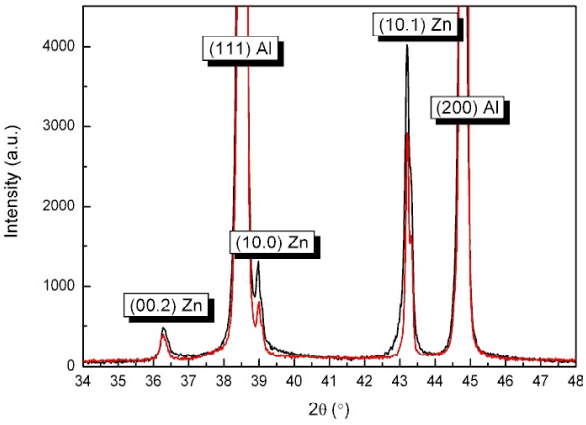

Fig. A2. XRD profiles of the Al-30Zn alloy after ECAP (black line) and after ECAP+SA (red line).